Carbon 103 (2016) 305–310

Contents lists available at ScienceDirect

Carbon

journal homepage: www.elsevier.com/locate/carbon

Contamination-free suspended graphene structures by a Ti-based transfer method

Alessia Matruglio [a, b, *], Silvia Nappini [b], Denys Naumenko [b], Elena Magnano [b, c], Federica Bondino [b], Marco Lazzarino [b], Simone Dal Zilio [b]

[a] University of Trieste, Graduate School of Nanotechnology, Piazzale Europa 1, 34127 Trieste, Italy
[b] IOM-CNR, Laboratorio TASC, S.S. 14-km 163.5, Basovizza, Trieste 34149, Italy
[c] Department of Physics, University of Johannesburg, PO Box 524, Auckland Park, 2006, Johannesburg, South Africa

ARTICLE INFO

Article history:
Received 22 December 2015
Received in revised form
18 February 2016
Accepted 11 March 2016
Available online 12 March 2016

ABSTRACT

Minimization of contamination associated with the graphene transfer process from the growth substrate to the device surface is a major requirement for large scale CVD graphene device applications. The most widespread transfer methods are based on the use of a thin sacrificial polymeric layer such as poly(-methyl methacrylate), but its complete removal after transfer is an unsolved problem; this issue is critical for suspended graphene, since the back surface often results contaminated by the dissolved polymer. Here we present a polymer-free method of commercial CVD-grown graphene transfer from the initial copper substrate to the silicon device, in which a 15 nm-thick titanium layer replaces completely the polymer film as supporting layer during the transfer process. Our approach reduces significantly the level of contaminations for supported and suspended graphene layers. Raman spectroscopy was used to prove the quality of the transferred graphene, not affected by this approach. X-ray photoelectron spectroscopy and X-ray absorption spectroscopy were used to assess the amount of the contaminants left by the transfer process. Overall carbon contamination was reduced by a factor 2, while contaminations originating from the metal etching in hydrofluoric acid, namely titanium and fluorine, were absent within the sensitivity of the used techniques.

1. Introduction

Since its first discovery in 2004 [1], graphene has attracted great interest because of its exceptional physical and chemical proprieties [2]. Such properties have opened the way for a wide variety of applications, including field-effect transistors [3,4], photonics and optoelectronics [5,6], energy production and storage [7–9], nanocomposite materials [10,11], biosensing [12,13]. Protocols for the production of high-quality and large-area graphene layers have been developed using Chemical Vapour Deposition (CVD) on transition-metal substrates, such as nickel (Ni) and copper (Cu) [14]. However, in order to integrate graphene on functional devices, these layers should be transferred from the growth substrate to the device surface, preserving graphene mechanical and chemical properties and avoiding contaminations. From the technological point of view, the transfer from the initial metal substrate to the final surface is still an open issue. Because of the easy handling and processing, the ideal transfer method is based on the use of a thin sacrificial polymer layer; the most commonly used is a layer of poly(methyl methacrylate) (PMMA) spin coated on the graphene. However the removal of PMMA residuals is still an unsolved problem [15] and it requires the use of high temperature annealing or other harsh protocols. Furthermore, graphene removed from rough metal is not completely flat and does not adhere perfectly to the device surface. The unattached regions are keener to become break points when the PMMA is dissolved away. In order to prevent cracks, the use of a second layer of PMMA has been proposed [16] but the thermal treatment of PMMA still leads to the creation of defects and in addition the residues are not completely eliminated [17]. Alternative transfer methods have been developed, such as dry-transfer process involving the use of a soft polymer such as polyethylene (LDPE and HDPE), polystyrene (PS), poly(lactide acid) (PLA) and poly(vinylidene-fluoride-co-trifluoroethylene) [18]: the polymer is put in contact with the graphene layer in low pressure

* Corresponding author. University of Trieste, Graduate School of Nanotechnology, Piazzale Europa 1, 34127 Trieste, Italy.
E-mail address: matruglio@iom.cnr.it (A. Matruglio).

http://dx.doi.org/10.1016/j.carbon.2016.03.023
0008-6223/

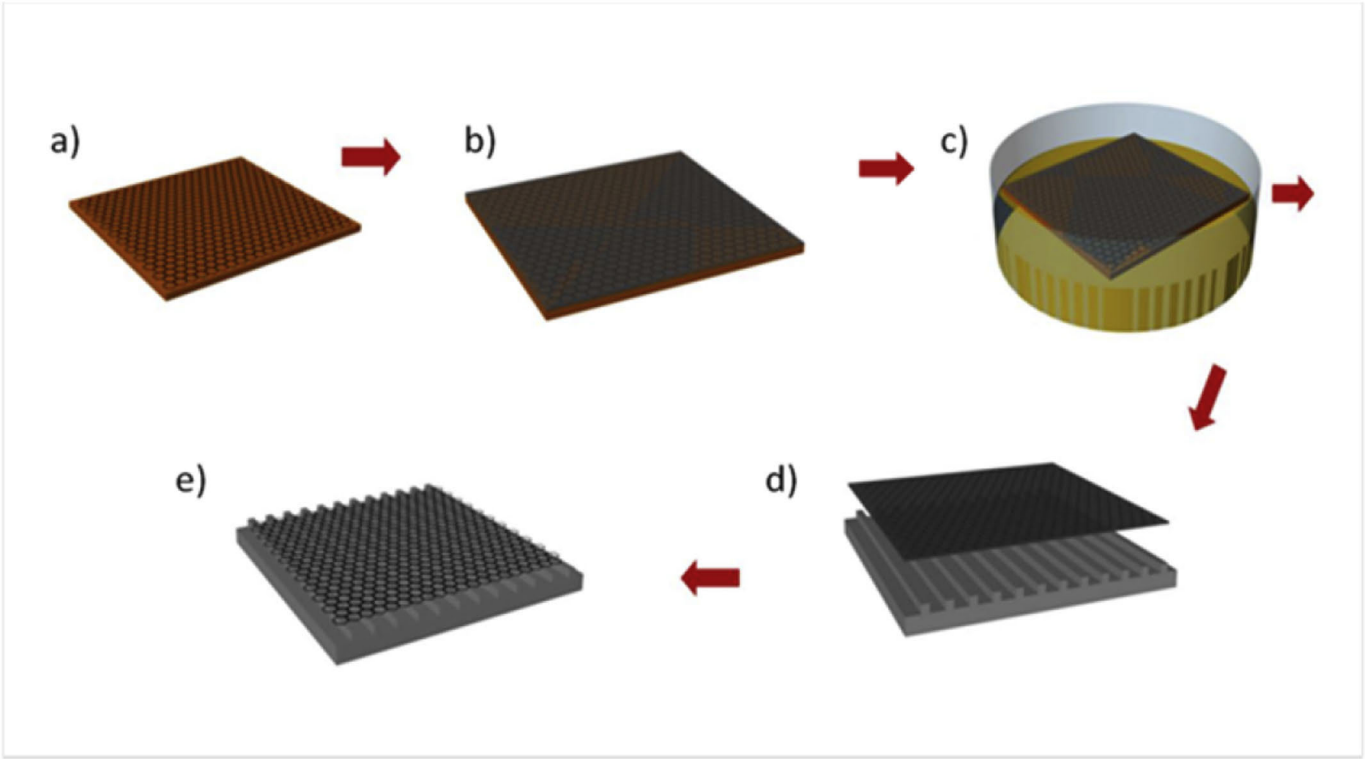

Fig. 1. Scheme of graphene transfer. a) CVD graphene on Cu foil; b) E-beam evaporation of 15 nm of Ti layer; c) wet etching of Cu; d) Gr/Ti transfer on Si substrate; e) graphene on Si substrate after Ti etching.(A colour version of this figure can be viewed online.)

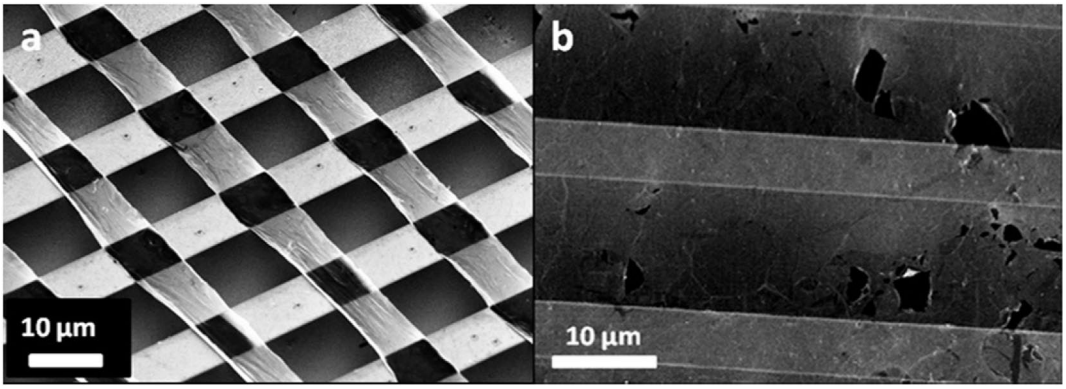

Fig. 2. SEM images of suspended graphene obtained with: (a) PG method using mr-I 7020 then removed with acetone. Graphene is patterned in stripes 10 μm long with plasma oxygen; graphene stripes are not transparent and this suggests strong contamination due to acetone and polymer visible on the back surface of suspended part. (b) MG method using a layer of Ti then removed in HF: graphene resulting after the Ti removal is clean; visible defects are propagated at grain boundaries.

conditions and graphene is peeled off the metal foil and transferred from the target substrate. Also polydimethylsiloxane (PDMS) stamps are commonly used for this purpose but graphene films show linear crack patterns after transfer [19]. Roll-to roll method permits transferring graphene layers using thermal release tape or polymer support, but the high quality of the as-grown graphene could be degraded during tape lamination and releasing [20]. More recently, the use of UV adhesive has been proposed [21], but this method induces a significant graphene doping therefore is not applicable where a fine control of the doping is required. An interesting approach to improve the cleaning of the surface has been provided by the use of a sacrificial titanium (Ti) layer deposited between graphene and PMMA [22]; the Ti coating avoids the direct contact of PMMA with the graphene, reducing carbon contamination. However, the Ti layer can be applied only to the exposed graphene side, while the side initially in contact with the growth substrate remains still unprotected; therefore when suspended graphene has to be produced, the back side of graphene still results contaminated by the dissolved PMMA.

Here we present a polymer-free method for commercial CVD-grown graphene transfer from Cu to a target substrate, which involves only the deposition of 15 nm layer of Ti directly on graphene. The absence of any polymeric supporting layer and the dissolution of Ti in hydrofluorhydric acid (HF) prevent the contamination of the back side of graphene, making the technique fast and suitable for both supported and suspended graphene layers. In order to develop and characterize our polymer-free transfer protocols, we produced several microstructured silicon substrates in which micrometric

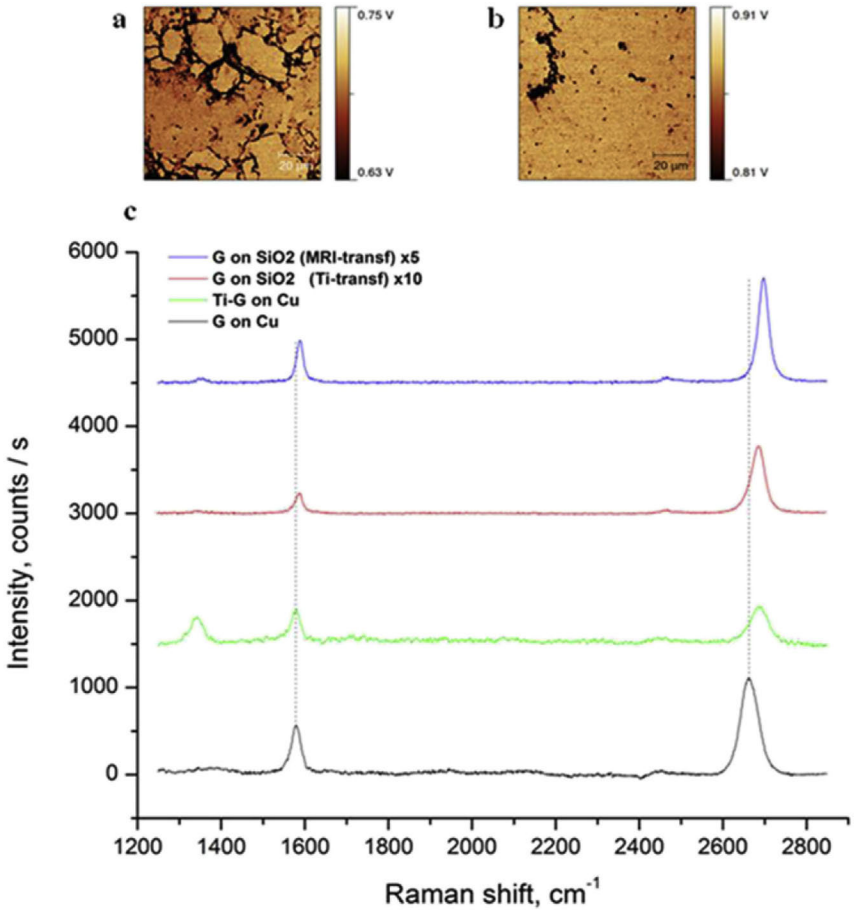

Fig. 3. LSC images of (a) PG sample and (b) MG sample. The dark parts indicate areas in which graphene is rolled up or in which defects or contamination are present, indicating that Ti-transfer produces a more uniform graphene layer; (c) Raman spectra of as-grown graphene acquired directly on Cu foil (black), covered by 15 nm thick Ti layer (green), and transferred on SiO_x/Si substrate using Ti (red) or mr-I 7020 (blue). The vertical black dotted lines are displayed for visual guidance and represent the positions of the G- and 2D-peaks of graphene. The excitation wavelength is 532 nm; the laser power on the sample is 1 mW.(A colour version of this figure can be viewed online.)

gratings were fabricated: the grating consisted of 10 μm-wide lines with a period of 20 μm. The grooves were deep etched in order to ensure full access to the etching solutions. Two transfer protocols were used for comparison, a conventional one based on a thermoplastic polymer (mr-I 7020) and the proposed, polymer free, one. The selection of mr-I 7020 instead of PMMA is motivated by its higher solubility in acetone that allows, in our experience, the production of cleaner graphene surfaces with respect simple PMMA: an example of transferred graphene with the two polymers obtained in our laboratory is shown in the section S1 of the Supplementary Information.

2. Materials and methods

2.1. Samples fabrication

The patterned substrates were produced on clean bulk silicon substrate by classical optical UV lithography technique. MICROPOSIT® S1803 photoresist is patterned with lines of width and periodicity of 10 μm and 20 μm, respectively. Inductively Coupled Plasma-Reactive Ion Etching (ICP-RIE) is used to transfer the pattern in the bulk silicon; ICP BOSCH® like process (gases: SF_6, C_4H_8, Ar) has been set in order to obtain a depth of 10 μm, followed by O2 plasma so as to remove the resist mask. 15 min in piranha solution (H_2SO_4:H_2O_2 7:3 ratio in volume) allows removing any residuals of carbon from the substrate. Commercial CVD-grown graphene on Cu foils purchased from Graphenea S.A. is used. A Scanning Electron Microscopy (SEM) image of the as-grown graphene is shown in the section S2 of the Supplementary Information.

Two transfer processes were tested using graphene from the same Cu foil in order to use graphene grown in the same conditions. For the first sample, labeled PG (Polymer-Graphene), a layer of 250 nm of mr-I 7020 (Micro Resist technology GmbH) is spin-coated on graphene. The Cu foil is subsequently etched overnight in Cu etching solution ($FeCl_3$:H_2O 3:7 ratio in volume). After the etching process, graphene is rinsed in DI water several times; the graphene transfer is done by fishing graphene into the water directly on the patterned substrate. Water is left to evaporate at room temperature for 2 h; mr-I 7020 is dissolved in cold acetone for 5 min. Critical point dryer (CPD) is performed in order to avoid the collapse of suspended graphene structures.

For the second sample, labeled MG (Metal-Graphene), we used our novel approach involving the deposition via electron-beam evaporation of a 15 nm-thick Ti layer on graphene with rate of 2 nm/s: the thickness was selected to be sufficient for supporting the graphene monolayer and preventing breakage. The transfer is leaded following the same protocol of the previous sample. Ti layer is removed in 1:10 HF:DI water solution for 2 min. CPD is performed also in this case in order to avoid the collapse of suspended graphene structures. A scheme of the process is shown in Fig. 1.

Fig. 2 shows SEM images of PG (Fig. 2a) and MG (Fig. 2b) samples: the film appears continuous on the scale of 10 μm, which is the size of the graphene crystalline grain obtained by CVD [23].

Above this size the formation of defects and cracks are observed due to the breaking at the grain boundaries, as already reported in literature [24,25].

Electrical measurements are performed in order to observe if the transfer method affects the graphene electrical proprieties. Bulk silicon with a thin thermal SiO_2 layer (300 nm) was used as substrate. Graphene is transferred according to the method used for PG sample and gold contacts are fabricated via electron beam evaporation on the top of graphene. The sheet resistance is measured in air on a surface area of $1900 \times 40\ \mu m^2$ using the transmission line method described in the reference [26]. The measured sheet resistance is equal to 2375 Ω/sq, higher than the value of 350 Ω/sq reported in the product datasheet [23]: this difference is ascribed to the size of the analyzed area. Indeed the average size of the crystalline domains is of the order 10 μm so that many high resistance grain boundaries are included and the resulting resistivity is higher. The same electrical measurements were not possible for the MG protocol because the use of HF metal etching solution removes the oxide; however, we expect the graphene resistivity to be dominated by grain boundary defects also in this case.

2.2. Sample spectroscopic analysis

Raman spectroscopy was performed on PG and MG samples produced on flat silicon substrates (SiOx/Si substrate). The measurements were performed in the reflection geometry on an inverted optical microscope (Axiovert 200, Zeiss) coupled with a 750 mm long spectrometer (Shamrock SR-750, Andor Technology plc). CW laser with the excitation wavelength of 532 nm (Cobolt Samba, 50 mW) was used. The light was focused on the sample by a 100x air objective (NA 0.8, EC Epiplan, Zeiss), resulting in a ~0.4 μm diameter laser spot. The laser power on the sample was controlled by variable neutral density filter and kept at 1 mW. Laser scanning confocal (LSC) microscopy was performed before the Raman measurements. To acquire the images of PG and MG samples, the reflected light was acquired with a femtowatt photoreceiver (New Focus, 2151, Newport Corp.) mounted on the second exit of the spectrometer. A dedicated electronics that controls a 100 μm by 100 μm piezo stage (JPK, Berlin) is finally used to the LSC images.

X-ray photoelectron spectroscopy (XPS) and X-ray absorption spectroscopy (XAS) measurements of both samples were performed at the CNR BACH beamline at Elettra synchrotron radiation facility in Trieste (Italy). The samples were annealed in ultra-high-vacuum conditions (UHV) for 1 h at 320 °C and with a flash at 380 °C with a base pressure $\leq 10^{-9}$ mbar. XPS spectra of C1s core level were acquired using an excitation energy set to 370 eV and a VG-Scienta R3000 hemispherical analyzer, working with an overall energy resolution of 0.2 eV.

Polarization-dependent Near-Edge-X-ray-Absorption Spectra (NEXAFS) was used to get information on the orbital hybridization and orientation of the graphene layer transferred on the silicon substrate. C K-edge NEXAFS were measured in partial electron yield mode (PEY) recording C KVV Auger using the electron energy analyzer fixed at the kinetic energy of 261 eV; Polarization-dependent NEXAFS spectra were measured with two different angles between polarization vector and surface plane: normal-incidence geometry ($\Theta = 0°$, s-polarization) and near-grazing incidence geometry ($\Theta = 60°$, p-polarization).

XAS spectra at the L_{23} edge of Ti and K edge of F were performed in total electron yield (TEY) method, in order to check possible residual traces of Ti and HF after metal etching.

3. Results and discussion

Raman spectrum of graphene exhibits few characteristic peaks described elsewhere [27,28]; we only note here that the D-peak can be observed if graphene symmetry is broken either by edges or defects [28] while the positions of G and 2D peak are sensitive to the graphene doping [29,30]. The representative LSC images of PG and MG samples are shown in Fig. 3a and Fig. 3b, respectively. Fig. 3c shows the Raman spectra of single-layer graphene CVD grown on Cu foil measured for different steps of transferring process on Si(100) terminated with a 2 nm thick native oxide layer: i) as-received; ii) covered by 15 nm-thick Ti layer; iii) transferred using the Ti sacrificial layer; iv) transferred using the mr-I 7020 sacrificial layer. The positions of the G and 2D peaks of graphene on Cu foil are centered at 1580 cm^{-1} and at 2665 cm^{-1}, and the 2D/G ratio is about 2. These are in a good agreement with the data already reported in the literature [31,32]. No distinguishable D peak is observed for graphene on Cu foil testifying its high quality; on the contrary an intense D peak is observed when 15-nm-thick Ti layer is deposited on graphene indicating the formation of defects after Ti deposition, the 2D peak is broadened and upshifted and the G/2D ratio is significantly decreased. This is qualitatively in agreement with that observed in literature [33]. The few quantitative differences observed (e.g. different G/2D ratio or the position of the 2D peak) can be justified observing that different substrates (e.g. metal vs dielectric ones) play an important role in graphene Raman response, however this is far beyond the scope of our experiments. More interestingly, after the transfer of Ti-supported graphene on SiO_x/Si substrate and the chemical removal of the Ti layer, graphene appears to recover the properties of the as grown one, as the position of the 2D peak remains the same; moreover, the D peak is again negligible testifying that all the defects induced by the Ti deposition are not permanent. When mr-I 7020 is used to transfer

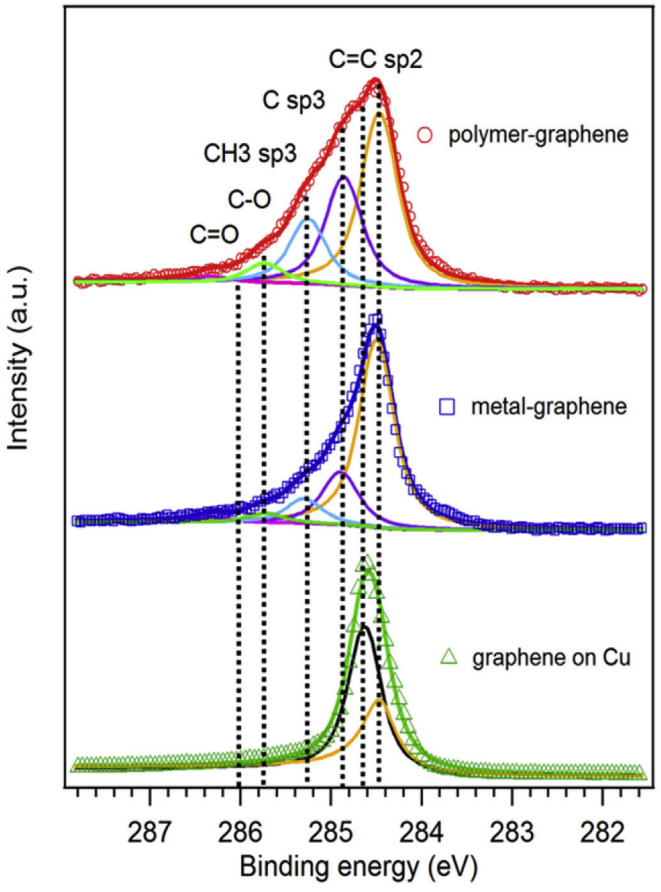

Fig. 4. C1s XPS spectra of PG (red curve), MG (blue curve) and graphene on Cu as grown (green curve).(A colour version of this figure can be viewed online.)

Table 1
Positions (eV) e areas (%) of peaks characteristic of C1s for MG, PG and graphene on Cu as-grown.

	C sp^2 (C=C)				C sp^3 (amorphous carbon)		C sp^3 (CH3)		C-O		C=O	
	Position (eV)		Area (%)		Position (eV)	Area (%)	Position (eV)	Area (%)	Position (eV)	Area (%)	Position (eV)	Area (%)
Ti	284.5		66.3		284.8	19.3	285.3	9.0	285.8	3.5	286.3	1.9
mr-I	284.5		46.7		284.8	28.9	285.3	17.4	285.8	5.3	286.3	1.7
Cu	284.5	284.65	36.3	63.7	–	–	–	–	–	–	–	–

graphene the D peak is more intense, 2D/G ratio is lower, and the position of the 2D peak is upshifted in comparison with Ti-transferred graphene. All these facts indicate that polymer traces are present on the surface of graphene after the removal while Ti-supported transfer is a cleaner approach.

The C1s XPS spectra for PG and MG samples are shown in Fig. 4. C1s peaks are fitted by a Voigt function, a symmetric convolution of Lorentzian lifetime and Gaussian instrumental broadening, after the subtraction of Shirley background to account for the inelastic photoelectrons. The main peak at 284.5 eV corresponds to the sp^2 carbon (C=C), distinctive of the pristine graphene. The presence of components at higher binding energy (BE) is a substantial signal of sp^3 hybridization, and other carbon functionalities, such as C–O and C=O [34,35] that can be due to physisorbed hydrocarbons. Two different components at 284.8 and 285.3 eV are ascribed to sp^3 species. More precisely: the peak at 284.8 eV is assigned to sp^3 in amorphous carbon and defects and could be due to the presence of grain boundaries and lattice defects [27], and also to defects introduced during the transfer mechanism [28] that can cause the formation of hydrogenated species at the boundaries, such as CH_3 groups (component at 285.3 eV) [29]. In PG sample the presence of hydrocarbon contaminants from polymer residuals further concur to increase the relative intensity of these components. Peaks at higher BE at 285.8 eV and 286.3 eV correspond to C–O and to C=O bonds, respectively; these oxidized states are given by the presence of chemisorbed oxygen that can be due to the prolonged exposure to atmospheric agents or to the transfer implemented in air [36]. Considering the ratio of the peak areas for each sample, these results show that in PG sample the peaks due to the sp^3 carbon and oxidized species (C–O, C=O) are more than twice as large than those obtained for MG one, suggesting that residues of polymer remain on graphene. Indeed, MG presents a lower contribution due to sp^3, C=O and C–O components, evidencing a sharp sp^2 carbon peak at 284.5 eV, which is distinctive of good quality pristine graphene. Spectra are compared with the C1s spectrum of as-grown graphene on Cu by CVD; this spectrum presents two components, the dominant one at 284.65 eV is the fingerprint of as-grown graphene on Cu that is shifted to higher BE with respect to graphene transferred on a substrate because of the stronger interaction with Cu that leads to n-doping as reported in literature [37]; the second feature at 284.65 eV could be associated to a weakly interacting component of graphene with Cu as a consequence of the possible decoupling between Cu and graphene in defected sites due to atmospheric agent exposure [37]. The position of the peaks and the corresponding areas are summarized in Table 1 for all samples.

In order to evaluate possible traces of Ti, XAS measurements are performed on MG sample after the etching of metal in HF. Fig. 5a shows the spectrum of Ti L_{23}-edge XAS and where no traces of Ti can be observed; a typical Ti spectrum is plotted (dashed line) taken from Ref. [38] for comparison. To estimate the minimal detectable Ti concentration, spectra of different known concentration of Ti were evaporated with the same parameters of MG sample. From the resulting calibration curve, we can estimate the amount of residuals Ti atoms to be below 2.3×10^{12} atoms/cm^2. More details are provided in the section S3 of the Supplementary Information. We also investigated the presence of fluorine (F) residues which could result from the HF solution: F K-edge XAS spectrum is shown in Fig. 5b: also in this case no F traces are present on graphene. A F 1s edge taken on a CaF_2 thick film with deposition of 1.2 nm of MnF_2 (dashed line) taken from Ref. [39] is plotted for comparison, demonstrating our approach as an alternative for an ultraclean graphene transfer method.

To further demonstrate the quality of the transferred graphene, polarization dependent C K-edge spectra NEXAFS was performed

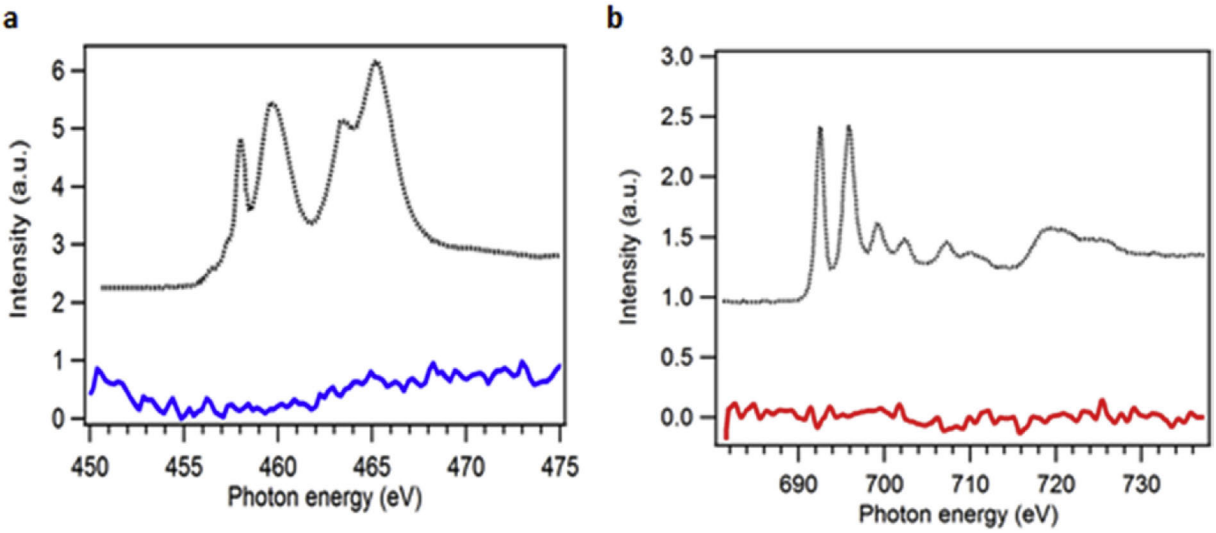

Fig. 5. XAS spectra of a) Ti L_{23}-edge of MG sample (blue line) compared with Ti L_{23} obtained on graphene transferred on TiO_2 (dashed line) taken from Ref. [38]; b) F k-edge on MG after Ti etching in HF (red line) compared with F 1s edge taken on a CaF_2 thick film after deposition of 1.2 nm of MnF_2 (dashed line) taken from Ref. [39].(A colour version of this figure can be viewed online.)

on MG sample, showing a graphene nearly flat, as described in section S4 of the Supplementary Information.

4. Conclusions

We have developed a graphene transfer method that involves only the interaction of CVD graphene with a thin Ti layer then removed in HF and avoids the use of any carbon-based supporting layer, usually polymers. The method is applicable to the fabrication of both supported and suspended graphene, and is particularly useful in the latter case, since the removal of Ti does not leave deposited residues on any side of the suspended graphene. Raman spectra showed that the quality of single-layer graphene transferred with Ti is not affected by the chemical and mechanical steps in the process; in particular we did not observe any change in graphene strain or any increase of the number of defects. XPS analysis showed that graphene transferred with our method is cleaner in comparison with graphene transferred with polymer. Raman analysis and XAS measurements confirm that our approach leaves no residue due to Ti or to Ti etching solution. Our approach opens up a new way to obtain high-quality transferred graphene for all fields of applications where pure graphene surface is required.

Acknowledgments

The work has partially founded by Italian Ministry of Education MIUR: grant n. FIRB Futuro in Ricerca 2012 RBFR128BEC “Beyond graphene: tailored C-layers for novel catalytic materials and green chemistry”; Progetto Premiale 2012' – Project ABNANOTECH and FIRB RBAP11ETKA “Approcci nanotecnologici per la teragnostica dei tumori”. Thanks to Stefano Roddaro and Rafaqat Hussain for the interesting conversations that have contributed to the development of this work.

Appendix A. Supplementary data

Supplementary data related to this article can be found at http://dx.doi.org/10.1016/j.carbon.2016.03.023.

References

[1] K.S. Novoselov, A.K. Geim, S.V. Morozov, D. Jiang, Y. Zhang, S.V. Dubonos, I.V. Grigorieva, A.A. Firsov, Electric field in atomically thin carbon films, Science 306 (5696) (2004) 666–669.
[2] M.J. Allen, V.C. Tung, R.B. Kaner, Honeycomb carbon: A review of graphene, Chem. Rev. 110 (1) (2010) 132–145.
[3] F. Schwierz, Graphene transistors, Nat. Nanotechnol. 5 (7) (2010) 487–496.
[4] Y.M. Lin, C. Dimitrakopoulos, K.A. Jenkins, D.B. Farmer, H.Y. Chiu, A. Grill, P. Avouris, 100-GHz Transistors from wafer-scale epitaxial graphene, Science 327 (5966) (2010) 662.
[5] Q.L. Bao, H. Zhang, Y. Wang, Z. Ni, Y. Yan, Z.X. Shen, K.P. Loh, D.Y. Tang, Atomic-layer graphene as a saturable absorber for ultrafast pulsed lasers, Adv. Funct. Mater. 19 (19) (2009) 3077–3083.
[6] K. Kim, J.Y. Choi, T. Kim, S.H. Cho, H.J. Chung, A role for graphene in silicon based semiconductor devices, Nature 479 (2011) 338–344.
[7] M.Q. Yang, N. Zhang, M. Pagliaro, Y.J. Xu, Artificial photosynthesis over graphene-semiconductor composites. Are we getting better? Chem. Soc. Rev. 43 (24) (2014) 8240–8254.
[8] N. Zhang, M.Q. Yang, S. Liu, Y. Sun, Y.J. Xu, Waltzing with the versatile platform of graphene to synthesize composite photocatalysts, Chem. Rev. 115 (18) (2015) 10307–10377.
[9] G. Srinivas, Y. Zhu, R. Piner, N. Skipper, M. Ellerby, R. Ruoff, Synthesis of graphene-like nanosheets and their hydrogen adsorption capacity, Carbon 48 (3) (2010) 630–635.
[10] S. Stankovich, D.A. Dikin, G.H.B. Dommett, K.M. Kohlhaas, E.J. Zimney, E.A. Stach, R.D. Piner, S.T. Nguyen, R.S. Ruoff, Graphene-based composite materials, Nature 442 (7100) (2006) 282–286.
[11] X. Huang, Z. Yin, S. Wu, X. Qi, Q. He, Q. Zhang, Q. Yan, F. Boey, H. Zhang, Graphene-based materials: synthesis, characterization, properties, and applications, Small 7 (14) (2011) 1876–1902.
[12] T.R. Nayak, H. Andersen, V.S. Maka, C. Kha, S. Bae, X. Xu, P.L.R. Ee, J.H. Ahn, B.H. Hong, G. Pastorin, B. Özyilmaz, Graphene for controlled and accelerated osteogenic differentiation of human mesenchymal stem cells, ACS Nano 5 (6) (2011) 4670–4678.
[13] T. Kuila, S. Bose, P. Khanra, A.K. Mishra, N.H. Ki, J.H. Lee, Recent advances in graphene-based biosensors, Biosens. Bioelectron. 26 (12) (2011) 4637–4648.
[14] Y. Zhang, L. Zhang, C. Zhou, Review of chemical vapor deposition of graphene and related applications, Acc. Chem. Res. 46 (10) (2013) 2329–2339.
[15] Y.C. Lin, C. Jin, J.C. Lee, S.F. Jen, K. Suenaga, P.W. Chiu, Clean transfer of graphene for isolation and suspension, ACS Nano 5 (3) (2011) 2362–2368.
[16] X. Li, Y. Zhu, W. Cai, M. Borysiak, B. Han, D. Chen, R.D. Piner, L. Colomba, R.S. Ruoff, Transfer of large-area graphene films for high-performance transparent conductive electrodes, Nano Lett. 9 (12) (2009) 4359–4363.
[17] G.B. Barin, Y. Song, I.D.F. Gimenez, A.G.S. Filho, L.S. Barreto, J. Kong, Optimized graphene transfer: influence of polymethylmethacrylate (PMMA) layer concentration and baking time on grapheme final performance, Carbon 84 (C) (2015) 82–90.
[18] G.J.M. Fechine, I. Martin Fernandez, G. Yiapanis, R. Bentini, E.S. Kulkarni, R.V. Bof De Oliveira, X. Hu, I. Yarovsky, A.H. Castro Neto, B. Özyilmaz, Direct dry transfer of chemical vapor deposition graphene to polymeric substrates, Carbon 83 (2015) 224–231.
[19] K.S. Kim, Y. Zhao, H. Jang, S.Y. Lee, J.M. Kim, K.S. Kim, J.H. Ahn, P. Kim, J.Y. Choi, B.H. Hong, Large-scale pattern growth of graphene films for stretchable transparent electrodes, Nature 457 (7230) (2009) 706–710.
[20] S. Bae, H. Kim, Y. Lee, X. Xu, J.S. Park, Y. Zheng, J. Balakrishnan, T. Lei, H. Ri Kim, Y.I. Song, Y.J. Kim, K.S. Kim, B. Özyilmaz, J.H. Ahn, B.H. Hong, S. Iijima, Roll-to-roll production of 30-inch graphene films for transparent electrodes, Nat. Nanotechnol. 5 (8) (2011) 574–578.
[21] Z. Shan, Q. Li, Z. Zhao, Z. Wang, Y. Wu, W. Cai, One-step transfer and doping of large area graphene by ultraviolet curing adhesive, Carbon 84 (C) (2015) 9–13.
[22] C.A. Joiner, T. Roy, Z.R. Hesabi, B. Chakrabarti, E.M. Vogel, Cleaning graphene with a titanium sacrificial layer, Appl. Phys. Lett. 104 (22) (2014) art. no. 223109.
[23] Available at: https://cdn.shopify.com/s/files/1/0191/2296/files/Graphenea_Monolayer_Film_Datasheet_2015-05-14.pdf?2328580123161991674.
[24] T.H. Liu, C.W. Pao, C.C. Chang, Effects of dislocation densities and distributions on graphene grain boundary failure strengths from atomistic simulations, Carbon 50 (10) (2012) 3465–3472.
[25] P.Y. Huang, C.S. Ruiz-Vargas, A.M. Van Der Zande, W.S. Whitney, M.P. Levendorf, J.W. Kevek, S. Garg, J.S. Alden, C.J. Hustedt, Y. Zhu, J. Park, P.L. McEuen, D.A. Muller, Grains and grain boundaries in single-layer graphene atomic patchwork quilts, Nature 469 (7330) (2011) 389–392.
[26] M. Lazzarino, T. Ozzello, G. Bratina, J.J. Paggel, L. Vanzetti, L. Sorba, A. Franciosi, Low resistance graded contacts to n-type ZnSe, Appl. Phys. Lett. 68 (3) (1996) 370–372.
[27] A.C. Ferrari, J.C. Meyer, V. Scardaci, C. Casiraghi, M. Lazzeri, F. Mauri, S. Piscanec, D. Jiang, K.S. Novoselov, S. Roth, A.K. Geim, Raman spectrum of graphene and graphene layers, Phys. Rev. Lett. 97 (2006) 187401.
[28] A.C. Ferrari, D.M. Basko, Raman spectroscopy as a versatile tool for studying the properties of graphene, Nat. Nanotechnol. 8 (4) (2013) 235–246.
[29] A. Das, S. Pisana, B. Chakraborty, S. Piscanec, S.K. Saha, U.V. Waghmare, K.S. Novoselov, H.R. Krishnamurthy, A.K. Geim, A.C. Ferrari, A.K. Sood, Monitoring dopants by Raman scattering in an electrochemically top-gated graphene transistor, Nat. Nanotechnol. 3 (4) (2008) 210–215.
[30] Q. Hao, S.M. Morton, B. Wang, Y. Zhao, L. Jensen, T. Jun Huang, Tuning surface-enhanced Raman scattering from graphene substrates using the electric field effect and chemical doping, Appl. Phys. Lett. 102 (1) (2013) art. no. 011102.
[31] O. Frank, J. Vejpravova, V. Holy, L. Kavan, M. Kalbac, Interaction between graphene and copper substrate: the role of lattice orientation, Carbon 68 (2014) 440–451.
[32] Y. Zhao, G. Chen, Y. Du, J. Xu, S. Wu, Y. Qu, Y. Zhu, Plasmonic-enhanced Raman scattering of graphene on growth substrates and its application in SERS, Nanoscale 6 (22) (2014) 13754–13760.
[33] M.W. Iqbal, A.K. Singh, M.Z. Iqbal, J. Eom, Raman fingerprint of doping due to metal adsorbates on graphene, J. Phys. Condens. Matter 24 (33) (2012) art. no. 335301.
[34] M.L. Ng, R. Balog, L. Hornekær, A.B. Preobrajenski, N.A. Vinogradov, N. Mårtensson, K. Schulte, Controlling hydrogenation of graphene on transition metals, J. Phys. Chem. C 114 (43) (2010) 18559–18565.
[35] M.J. Webb, P. Palmgren, P. Pal, O. Karis, H. Grennberg, A simple method to produce almost perfect graphene on highly oriented pyrolytic graphite, Carbon 49 (2001) 3242–3249.
[36] N. Peltekis, S. Kumar, N. McEvoy, K. Lee, A. Weidlich, G.S. Duesberg, The effect of downstream plasma treatments on graphene surfaces, Carbon 50 (2) (2012) 395–403.
[37] P.R. Kidambi, B.C. Bayer, R. Blume, Z.J. Wang, C. Baehtz, R.S. Weatherup, M.G. Willinger, R. Schloegl, S. Hofmann, Observing graphene grow: catalyst-graphene interactions during scalable graphene growth on polycrystalline copper, Nano Lett. 13 (10) (2013) 4769–4778.
[38] M. Favaro, S. Agnoli, C. Di Valentin, C. Mattevi, M. Cattelan, L. Artiglia, E. Magnano, F. Bondino, S. Nappini, G. Granozzi, TiO2/graphene nanocomposites from the direct reduction of graphene oxide by metal evaporation, Carbon 68 (2014) 319–329.
[39] L. Pasquali, G. Selvaggi, M. Montecchi, A.G. Banshchikov, A.K. Kaveev, S.M. Suturin, N.S. Sokolov, F. Borgatti, B. Doyle, A. Giglia, N. Mahne, M. Pedio, S. Nannarone, St Petersburg, Russia, in: X-Ray Absorption and Reflectivity Studies of MnF2 Initial Growth on CaF2/Si(111.) in 12th International Symposium NANOSTRUCTURES: Physics and Technology, June 21-25, 2004, pp. 48–50. literal.